ISSN: 2319-5967
ISO 9001:2008 Certified
International Journal of Engineering Science and Innovative Technology (IJESIT)
Volume 3, Issue 4, July 2014

Polarimetric Hyper spectral Imaging: Analysis, Modeling and Simulation

Supriya P. Gaikwad[1], Vijay R. Dahake[2]
[1]P.G Student, [2]Professor,
Ramrao adik institute of technology, Nerul, Navi Mumbai-410210. India.

Abstract:- ***The work on polarimetric hyper spectral imaging mechanism and on image characteristics is of great importance for information extraction and utilization of the images. Polarimetric hyper spectral images can provide spectral, spatial, and polarimetric information of a scene, which are unique and comprehensive for remote sensing applications such as growth monitoring of crops, analysis of water quality, and geology mapping, etc. The purpose is to analyze the mechanism of polarimetric hyper spectral imaging and to model such a process. The outcome will help designers and users of a polarimetric hyper spectral imaging system to further understand the system and take full advantages of it. Here, a polarimetric hyper spectral imaging model is proposed, in which the influence of skylight on polarization is considered, Hyper spectral images contain a wealth of data, Hyper spectral imaging (HSI) systems can acquire both spectral and spatial information of ground surface simultaneously and have been used in a variety of applications such as object detection, material identification, land cover classification etc. Here we analyze and calculate the condition and parameters of the imaging models, the uniqueness, and usefulness of the integration of polarimetric and spectral information. we generate the polarimetric hyper spectral image data source according to the imaging model. The polarimetric hyper spectral image model here is realized at the low attitude considering the characteristic of atmosphere environment.***

***Keywords*-Imaging modelling, polarimetric hyper spectral images, polarimetric information, image simulation.**

I. INTRODUCTION

Hyper spectral imaging belongs to a class of techniques commonly referred to as spectral imaging or spectral analysis. Hyper spectral imaging is the collecting and processing of information from across the electromagnetic spectrum. A simple analogy to understand the concept of hyper spectral imaging better- the human eye sees visible light in three bands, i.e. red, green, and blue whereas spectral imaging divides the spectrum into many more bands. The modeling of hyper spectral imaging systems plays a number of roles in the development and application of the technology. One primary role is that by constructing and validating models, we demonstrate our understanding of the problematics and processes of hyper spectral imaging. Another major role is to create accurate simulations of hyper spectral images, which can be used as test imagery for algorithm development. A third role is to optimize the design and operation of the imaging systems by allowing trade off studies to characterize the impact of system parameter choices.

The research on polarimetric hyper spectral imaging mechanism and on image characteristics is of great importance for further information extraction and utilization. In this project we analyze the mechanism of polarimetric hyper spectral imaging and model such a process. The outcome of the work can help system designers and users understand imaging process better and find the influencing factors to system performance, so as to optimize sensor parameters and to plan new missions. Hyper spectral images possess spectral and spatial information of ground cover, which have been widely used in remote sensing fields. Polarimetric hyper spectral images can provide extra polarimetric information of a scene and are expected to play more important role than hyper spectral images in remote sensing applications such as monitoring growth status of vegetation [15], the atmosphere [16], and underwater ecological environment [17], etc. A hyper spectral remote sensing system is designed to faithfully represent the whole imaging process on the premise of reduced description complexity. It can help system users understand the hyper spectral imaging (HSI) system better and find the key contributors to system performance so as to design more advanced hyper spectral sensors and to optimize system parameters. A great number of efficient and cost-effective data can also be produced for validation of hyper spectral data processing. As both sensor and processing systems become increasingly complex, the need for understanding the

ISSN: 2319-5967
ISO 9001:2008 Certified
International Journal of Engineering Science and Innovative Technology (IJESIT)
Volume 3, Issue 4, July 2014

impact of various system parameters on performance also increases. Hyper spectral images contain a wealth of data, interpreting them requires an understanding of exactly what properties of ground materials we are trying to measure, and how they relate to the measurements actually made by the hyper spectral sensor.

II. LITERATURE SURVEY

Many researches on modeling of hyper spectral imaging process [20] have been carried out. As early as 1989, Kerekes and Landgrebe made a detailed description about the modeling and simulation of optical remote sensing system [21]. Up to now, many models are developed to describe the reflection of vegetation canopies, such as AGR model [12], Suits model [6], etc.

SAIL (scattering by arbitrary inclined leaves) is one of the earliest canopy reflectance models [7], which is now widely applied in remote sensing community and gives rise to several improved versions. Kuusk put forward an improved SAIL model where the hot-spot effect was added [1]. Recently, Verhoef. Proposed an extension of GeoSAIL including crown clumping, which was additiveally combined with PROSPECT(a model of leaf optical properties spectra) and a soil BRDF (bidirectional reflectance distribution function) model [14]. Fast canopy reflectance (FCR) model [9] overcomes the defect of SAIL model that failed considering the specular reflection on leaf surfaces and the hot-spot effect, which is the successor to Nilson and Kuusk's (N-K) [10] and Verhoef's SAIL models, and thus has the precision of the N-K model and the speed of the SAIL model. The four-stream model is applied to describe the complex interaction of the heterogeneous and non-Lambertian land surface with the atmosphere in an effective manner. The six atmosphere parameters of four stream model can be calculated by MODTRAN4.0. Vanderbilt and Grant firstly derived a specular reflectance and polarized reflectance model for the headed and preheaded plant canopy [19]. Rondeaux and Herman put forward a polarized reflectance model for vegetation canopy accounting for leaf angle distribution [2]. Subsequently, Breon proposed a simpler version which assumes a random leaf orientation for vegetation canopy and bare soil. However, Breon's models do not contain any empirical parameter, so Nadal come up with a semi-empirical model with two empirical coefficients that are determined by the normalized difference vegetation index of the observed surface. In 2005, Shell further analyzed three backgrounds and six targets polarization in his doctoral dissertation. In 2009, Waquet presented an alternative to the previous model by using a shadowing function given by Saunders, which assumed a Gaussian distribution of the surface slopes. In the same year, Maignan also proposed a general model which gave very satisfactory results for many surfaces.

III. MODELS FOR MODELING OF HYPERSPECTRAL IMAGING

A. Polarized reflectance model

Polarization mainly comes from the specular reflection of sunlight, although polarimetric information produced by skylight should not be ignored. Polarized radiance basically comes from the microcosmic surface's specular reflection, and these microcosmic surfaces are small Fresnel's reflectors with random orientation. As shown in Figure 1, it is evident that the microscopic normal and macroscopic normal are not consistent. When the ground target's surfaces are flat or near flat, their microscopic normal's are almost parallel to the macroscopic normal. Under this condition, the microscopic normal often obeys a certain distribution function like Gaussian distribution, and the function's center is the macroscopic normal. More precisely, let S and dS stand, respectively, for macroscopic surface and for microcosmic surfaces whose direction of the normal is (μ_n, φ_n) within $d\omega_n$. dS represents the project of microcosmic surface dS_0. Then, the microcosmic surface's normal is characterized by the distribution function $p(\mu_n, \varphi_n)$ such that.

$$p(\mu_n, \varphi_n)\, d\omega_n = dS/S \quad \ldots\ldots(1)$$

We can derive the polarized radiance L^{up} as,

$$L^{up} = \frac{E_p(\mu_n, \varphi_n)}{4\mu_v \mu_n} F_p(i,n) \quad \ldots\ldots(2)$$

And the value of polarized reflectance R_{pol} can be deducted by,

$$R_{pol}(i) = \frac{\pi \times p(\mu_n, \varphi_n)}{4\mu_v \mu_n \mu_s} F_p(i,n) \quad \ldots\ldots(3)$$

ISSN: 2319-5967
ISO 9001:2008 Certified
International Journal of Engineering Science and Innovative Technology (IJESIT)
Volume 3, Issue 4, July 2014

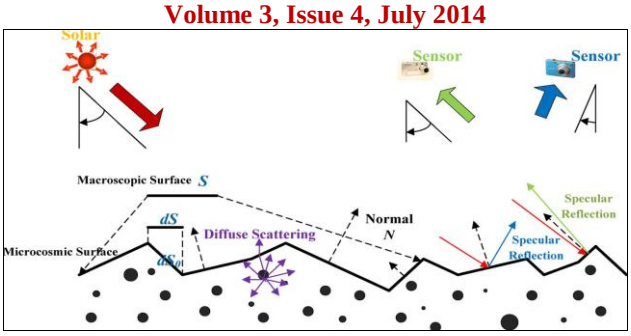

Fig 1 Propagation of light

In general, $p(\mu_n, \varphi_n)$ can be regarded as a Gaussian function, $F_p(i, n)$ is Freshnel's polarized reflection coefficient. As the specular reflection is highly dependent on the types of material, surface roughness, etc., here we just consider the condition that surfaces are relatively flat; thus, the direction of surface's specular reflection is close to that of macroscopic normal's specular reflection. In this instance, when the microscopic normal is parallel to the macroscopic normal, incident light is reflected in the direction that reflected angle is equal to the incident angle; incident light and reflected light are within some plane according to Fresnel principle. This phenomenon is stochastic; the probability will gradually decrease when the microscopic normal is far from the macroscopic normal.

a) Case of vegetation: - A simple polarized reflectance model for vegetation canopy was proposed by Rondeaux and Herman in 1991. This model accounts for the leaf angle distribution and analyzes the effect of light transmission through the canopy. They pointed that the polarized reflectance is independent on the leaf area index for a dense canopy (LAI $\geq$ 3) Breon put forward a simpler version of the polarized reflectance model for vegetation canopy, which assumes a uniform leaf orientation and ignores the effect of LAI [3]. Leaf angle distribution function is generally defined as the probability density of leaf angle. Breon's vegetation canopy model results are often lower than the measured data. Hence, we adopt the Rondeaux-Herman model in our work, and the effect of LAI is ignored. The SAIL model is an improved version of Suits's canopy reflectance model.

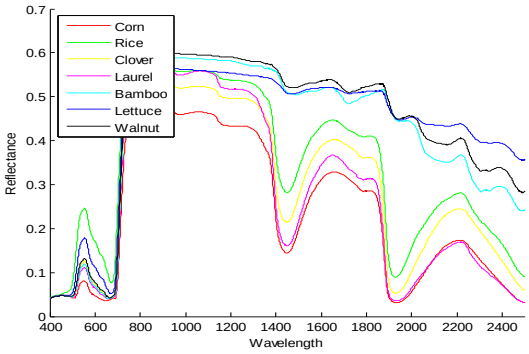

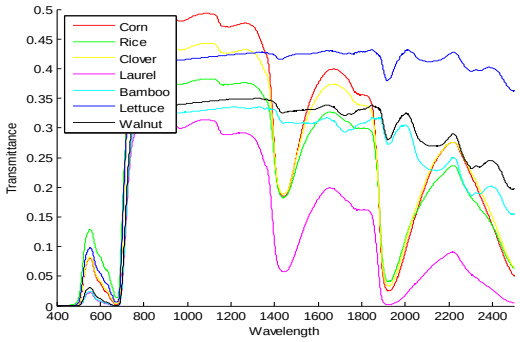

Fig 2 Reflectances for different vegetation canopy **Fig 3 transmittances for different vegetation canopy**

Figures 2 & 3 shows reflectances and transmittances for different vegetation canopies respectively.

b) Case of top soil:- A polarized reflectance model for bare soils was also given by Breon, using the hypothesis like that for vegetation canopy. Moreover, it does not consider attenuation of the incoming reflected rays within the depth of the canopy. The top soil model results are often higher than the measured data [4]. Waquet introduced a polarized reflectance model using a shadowing function, and this model fit not only for vegetation surface but for bare soils [11]. From figure 4 we can see that the polarized reflectance decreases with the increase of roughness factor. It is because the rougher the surface, the more severe attenuation of flux.

c) Case of water surface: - The water's polarized reflectance is affected by the waves, which depends on the wind speed. Hence, a wave facet's distribution function derived by Cox and Munk depends only on the wind

ISSN: 2319-5967
ISO 9001:2008 Certified
International Journal of Engineering Science and Innovative Technology (IJESIT)
Volume 3, Issue 4, July 2014

speed ω and preserves the symmetry of the reflectance law [13]. The model assume that the entire water surface or some part of the land surface consists in small Fresnel's reflectors with random orientation. From figure 5 we observe that the value of polarized reflectance is also influenced by the climate, so the polarization can be utilized to monitor the weather change.

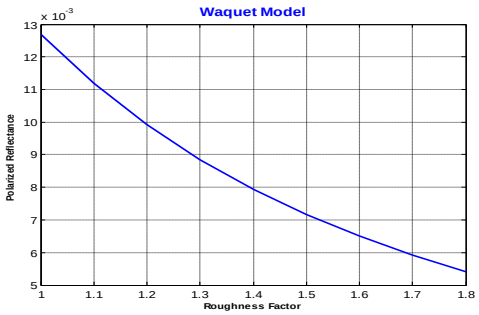

Fig 4 Waquet model

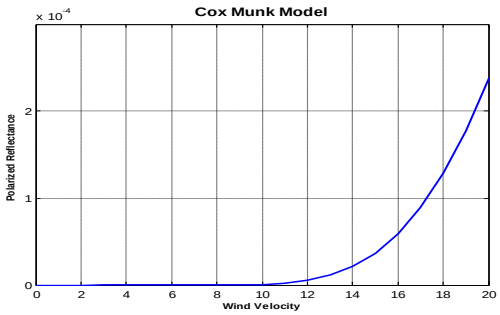

Fig 5 Cox-Munk model

IV. IMPLEMENTATION OF POLARIMETRIC HYPERSPECTRAL IMAGING

This project proposes a polarimetric hyper spectral imaging model, in which the influence of skylight on polarization is considered. A model of polarimetric hyper spectral imaging process based on the previous work of hyper spectral image modeling, and polarimetric information is characterized and introduced in the model. In contrast with the previous hyper spectral image modeling, however, the polarimetric hyper spectral image model here is realized at the low attitude considering the characteristic of atmosphere environment. Finally we also analyze the sub pixel model.

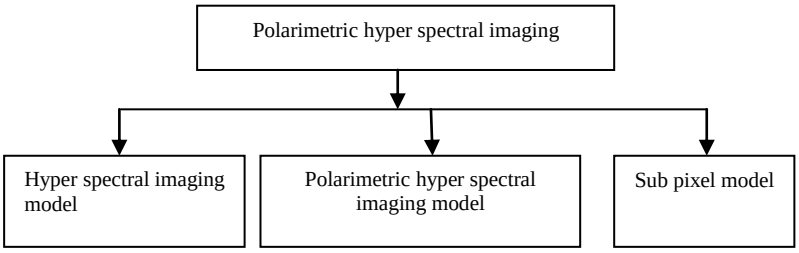

Fig 6-Implementation of polarimetric hyper spectral imaging

A. Polarimetric hyper spectral imaging

Based on our previous the hyper spectral simulation work augments the polarization part. Therefore, we first analyze the hyper spectral imaging model and then put forward the polarimetric hyper spectral imaging model.

1) Hyper spectral imaging model

In the modeling of hyper spectral imaging process, the four-stream radiance model [8] is adopted, in which major effects including heterogeneity of landscape, non- Lambertian reflectance of the land surface, atmospheric adjacency effect, and the limited spatial resolution of instrument are considered. The four-stream approximation is a reasonable tradeoff between real case and computational efficiency. In the model, the integral of equation needs to be determined to compute the radiance L_o of a surface element in observer's direction.

$$L_o(\mu_o,\varphi_o) = \rho(\mu_o,\varphi_o,\mu_s,\varphi_s)\, E_s(\mu_s,\varphi_s) + \int_0^{2\pi}\int_0^{1} \rho(\mu_o,\varphi_o,\mu_i,\varphi_i)\, L_i(\mu_i,\varphi_i)\, \mu_i\, d\mu_i\, d\varphi_i \quad \ldots\ldots\ldots\ldots\ldots\ldots(4)$$

Where L_o is the radiance to the observer, ρ is the four dimensional BRDF, Es is the direct solar irradiance on a horizontal plane, μ (cosine of the zenith angle) and φ (azimuth) are directional arguments for directions signed by subscripts: s (from the sun), i (from the sky), and o (to the observer). According to the four-stream radioactive transfer theory, the radiance Lo received by the sensor can be computed as,

ISSN: 2319-5967
ISO 9001:2008 Certified
International Journal of Engineering Science and Innovative Technology (IJESIT)
Volume 3, Issue 4, July 2014

$$L_o = \rho_{so}\frac{E_s^o}{\pi}\cos\theta_s + \frac{\tau_{ss}\bar{r}_{sd}+\tau_{sd}\bar{r}_{dd}}{1-\bar{r}_{dd}\rho_{dd}}\tau_{do}\frac{E_s^o}{\pi}\cos\theta_s + \frac{\tau_{sd}+\tau_{ss}\bar{r}_{sd}\rho_{dd}}{1-\bar{r}_{dd}\rho_{dd}}r_{do}\tau_{oo}\frac{E_s^o}{\pi}\cos\theta_s + \tau_{ss}r_{so}\tau_{oo}\frac{E_s^o}{\pi}\cos\theta_s \quad \text{.....(5)}$$

where r_{so} is target bidirectional reflectance, r_{do} is target directional reflectance for diffuse incidence, r_{sd} is the average surroundings diffuse reflectance for solar incidence, r_{dd} is the average surroundings diffuse reflectance for diffuse incidence, ρ_{so} is the bidirectional reflectance at the top of atmosphere, ρ_{dd} is the spherical albedo at the bottom of atmosphere (BOA), τ_{ss} is the direct atmospheric transmittance in the direction of the sun, τ_{oo} is the direct atmospheric transmittance in the direction of viewing, τ_{sd} is the diffuse atmospheric transmittance for solar incidence, τ_{do} is the directional atmospheric transmittance for diffuse incidence, E_{os} is the direct solar irradiance on a plane perpendicular to the sunrays, and θ_s is the local solar zenith angle. According to the theory of Verhoef's four stream model, we rederive the model again. The six atmosphere parameters calculated are,

$$\tau_{ss} = \exp(-b/\cos\theta_s) \quad \text{.....(6)}$$

$$\tau_{oo} = \exp(-b/\cos\theta_o) \quad \text{.....(7)}$$

$$\tau_{ss}\tau_{oo} = \exp[-b(1/\cos\theta_s + 1/\cos\theta_o)] = GSUN_{100}\times\pi/(E_s^o\cos\theta_s) \quad \text{.....(8)}$$

$$\rho_{so} = PATH_o\times\pi/(E_s^o\cos\theta_s) \quad \text{.....(9)}$$

$$\tau_{sd} = \left[\frac{GTOT_{100}(1-\rho_{dd})}{GSUN_{100}} - \rho_{dd}\right]\tau_{ss} \quad \text{.....(*)(10)}$$

$$\tau_{do} = \frac{PATH_{100}-PATH_0}{GTOT_{100}}\cdot\frac{\tau_{sd}+\tau_{ss}\rho_{dd}}{\tau_{sd}+\tau_{ss}}\tau_{oo} \quad \text{.....(*)(11)}$$

$$\rho_{dd}^2\left(\frac{GTOT_{50}}{GTOT_{100}}-\frac{1}{2}\right)\tau_{ss} + \rho_{dd}\left[\frac{\tau_{ss}}{2}-\tau_{sd}+(\tau_{sd}-2\tau_{ss})\cdot\frac{GTOT_{50}}{GTOT_{100}}\right] + \left(1-2\cdot\frac{GTOT_{50}}{GTOT_{100}}\right)\cdot\tau_{sd} = 0 \quad \text{.....(*)(12)}$$

Where b is the extinction coefficient representing the optical thickness of the atmospheric layer, and θ_o is the zenith angle of observation. $GTOT_0$, $GTOT_{50}$, and $GTOT_{100}$ are spectrally flat surface albedos of 0%, 50%, and 100%, respectively; here all for a uniform Lambertian surface reflectance. The three revised parameter equations are labeled by (∗) including the diffuse atmospheric transmittance for solar incidence τ_{sd}, the directional atmospheric transmittance for diffuse incidence τ_{do}, and the BOA spherical albedo of the atmosphere ρ_{dd}. After the six atmosphere parameters are obtained, and the four directional reflectance parameters also can be calculated. The results of six atmosphere parameters are shown in Fig. 8. are obtained by three MODTRAN runs. The three runs, are all for a uniform Lambertian surface reflectance, with spectrally flat surface albedos of 0%, 50%, and 100%, respectively

2) Polarimetric hyper spectral imaging model

Polarized radiance mainly depends on the specular reflection of sunlight; thus, conventional surface polarized radiance model does not take the skylight into consideration. However, the contribution of skylight for polarized radiance cannot be ignored. According to the data which is obtained [5], the ratio of polarized radiance which is produced by skylight is in the range of 10%–20%. Therefore, we need to integrate the polarized radiance from skylight.

By means of a flux-interaction diagram, the radiative transfer inside the atmosphere and the non-Lambertian reflection at the earth's surface can be summarized as in Figure 7. According to the four-stream model, the total radiance received by sensor is L_o. Then, the total radiance is divided into five parts which are path radiance, adjacent radiance, ref-sun radiance, ref-multi-skylight radiance, and ref-Rayleigh radiance.

ISSN: 2319-5967
ISO 9001:2008 Certified
International Journal of Engineering Science and Innovative Technology (IJESIT)
Volume 3, Issue 4, July 2014

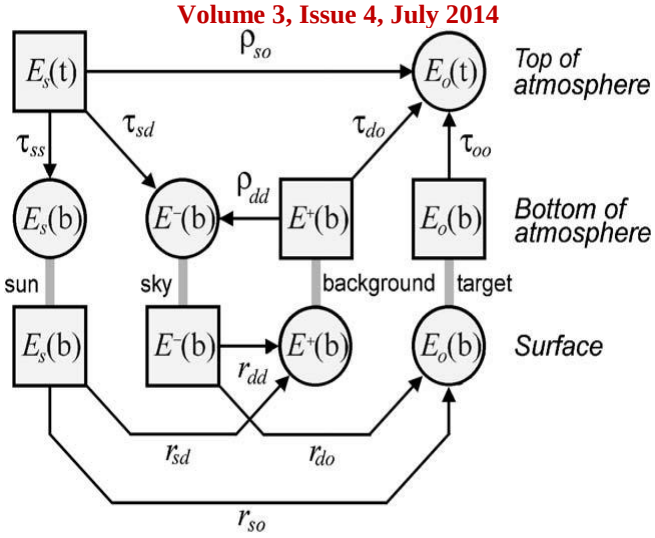

Fig 7. Flux-interaction diagram of the atmosphere over a non-Lambertian reflecting earth's surface

The "ref-" means that the ground target reflects incident light, and incident light may be sunlight (ref-sun), or multiple scattering skylight (ref-multi-skylight), or skylight from Rayleigh scattering (ref-rayleigh).

$$L_o = L_{path} + L_{adjacent} + (L_{mul-scattering} \cdot r_{do} + L_{reyleigh} \cdot r_{do} + L_{sun} \cdot r_{so})\tau_{oo} \text{.....(13a)}$$

$$L_o = \rho_{so}\frac{E_s^o}{\pi}\cos\theta_s + \frac{\tau_{ss}\bar{r}_{sd} + \tau_{sd}\bar{r}_{dd}}{1-\bar{r}_{dd}\rho_{dd}}\tau_{do}\frac{E_s^o}{\pi}\cos\theta_s + \frac{\tau_{sd}\bar{r}_{dd} + \tau_{ss}\bar{r}_{sd}}{1-\bar{r}_{dd}\rho_{dd}}\rho_{dd}\frac{E_s^o}{\pi}\cos\theta_s \cdot r_{do}\tau_{oo} + \tau_{sd}\frac{E_s^o}{\pi}\cos\theta_s \cdot r_{do}\tau_{oo} + \tau_{ss}\frac{E_s^o}{\pi}\cos\theta_s \cdot r_{so}\tau_{oo} \text{.....(13b)}$$

Where, L_{path} and $L_{adjancet}$ received by sensor, are path radiance and adjacent radiance. $L_{mul-scattering}$, $L_{rayleigh}$, and L_{sun} are radiances from multiple scattering skylights, skylight from Rayleigh scattering, and sunlight that irradiate into the target.

Moreover, it is reasonable that Waquet ignores the path polarized radiance and adjacent polarized radiance when the weather is "no rain, no cloud," and the altitude of sensor is lower than 35 km. The atmospheric polarized radiance can be accurately estimated using the successive order of scattering code. To simplify, we also ignore the path polarized radiance and adjacent polarized radiance. Therefore, in terms of polarized radiance, we just consider that the polarized radiance comes from ground targets.

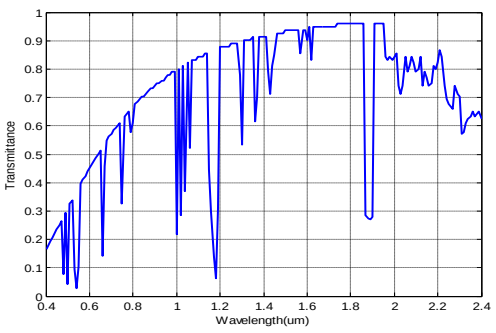

(a)

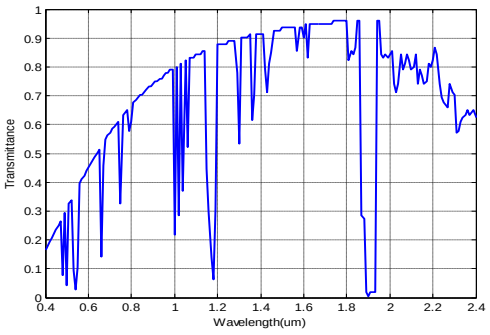

(b)

ISSN: 2319-5967
ISO 9001:2008 Certified
International Journal of Engineering Science and Innovative Technology (IJESIT)
Volume 3, Issue 4, July 2014

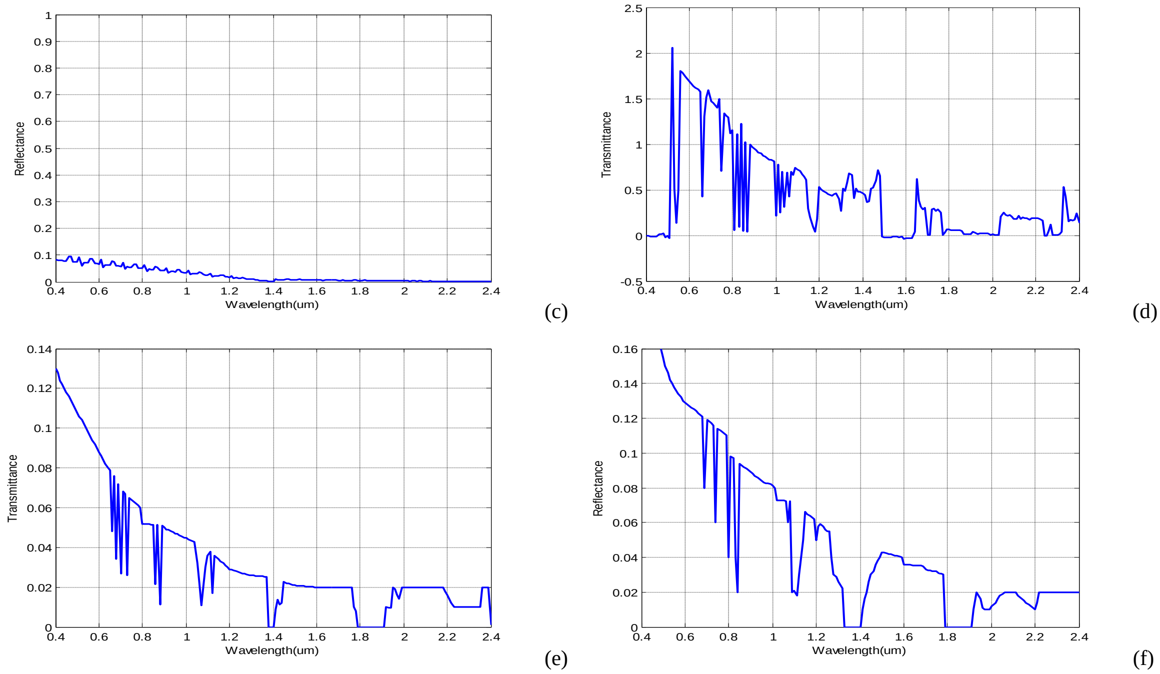

Fig 8. Six atmosphere parameters (a) τ_{ss} (b) τ_{oo} (c) ρ_{so} (d) τ_{sd} (e) τ_{do} (f) ρ_{dd}.

3) Sub pixel Model

Here, a simple area-weighted linear mixing model is used to obtain the reflectance of pixels in woodland-road scene that contains two classes (shrubbery and uncovered soil). Particularly, for cylindrical and spherical plant crown, according to the interaction between the crown and ground surface geometric-optical characteristics, four ground surface fractions can be decided. A pixel is modeled as an area-weighted sum of the reflectance of the four scene components: sunlit ground, sunlit crown, shadowed ground, and shadowed crown. The reflectance of mixed pixel in the scene depends on the four parameters, i.e., f_C for sunlit crown, f_T for shadowed crown side, f_G for sunlit ground, and f_Z for shadowed ground. The four sub pixel parameters are used to describe the proportion of the four representative scene components, respectively, which are influenced by solar zenith angle, viewing zenith angle, and tree density per resolution element in the scene. This sub pixel model has been described [18].

1) Directional Reflectance Parameters: For the sub pixel model, the directional reflectance r_{so}, r_{do}, r_{sd}, and r_{dd} are,

$$r_{so} = f_C \rho_c(\mu_o, \varphi_o, \mu_s, \varphi_s) + f_G \rho_s(\mu_o, \varphi_o, \mu_s, \varphi_s) \quad (14)$$

$$r_{do} = \frac{1}{\pi} \int_0^{2\pi} \int_0^1 [(f_C + f_T)\rho_c(\mu_o, \varphi_o, \mu_i, \varphi_i) + (f_G + f_Z)\rho_s(\mu_o, \varphi_o, \mu_i, \varphi_i)]\, \mu_i\, d\mu_i\, d\varphi_i \quad (15)$$

$$r_{sd} = \frac{1}{\pi} \int_0^{2\pi} \int_0^1 [f_C \rho_c(\mu_i, \varphi_i, \mu_s, \varphi_s) + f_G \rho_s(\mu_i, \varphi_i, \mu_s, \varphi_s)]\, \mu_i\, d\mu_i\, d\varphi_i \quad (16)$$

$$r_{dd} = \frac{1}{\pi^2} \int_0^{2\pi} \int_0^1 \int_0^{2\pi} \int_0^1 [(f_C + f_T)\rho_c(\mu_o, \varphi_o, \mu_i, \varphi_i) + (f_G + f_Z)\rho_s(\mu_o, \varphi_o, \mu_i, \varphi_i)] \times \mu_i \mu_o\, d\mu_i\, d\varphi_i\, d\mu_o\, d\varphi_o \quad (17)$$

The foliage's reflectance $\rho_c(\mu_o, \varphi_o, \mu_s, \varphi_s)$ is realized by FCR model. The soil can be seen as Lambertian surface, whose reflectance $\rho_s(\mu_o, \varphi_o, \mu_s, \varphi_s)$ can be obtained from the spectrum database.

ISSN: 2319-5967
ISO 9001:2008 Certified
International Journal of Engineering Science and Innovative Technology (IJESIT)
Volume 3, Issue 4, July 2014

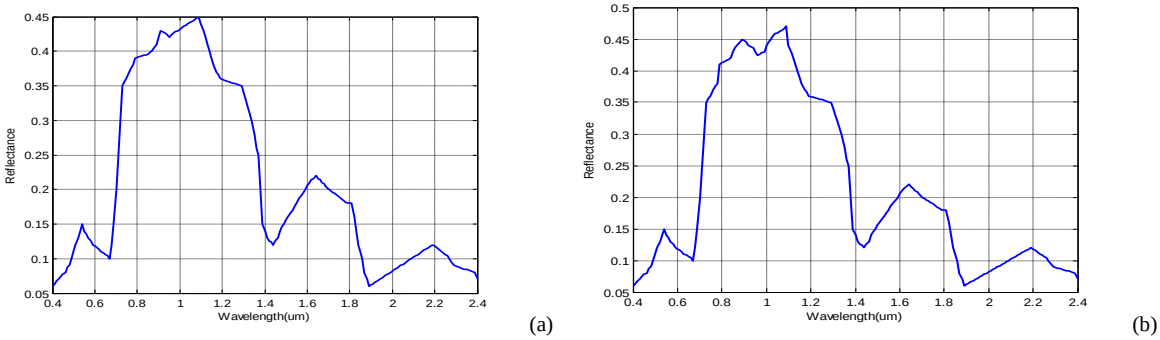

(a) (b)

Fig 9 four directional reflectance parameters (a) r_{so} (b) r_{do}.

The results of two directional reflectance parameters are shown in Fig. 9. Like this the remaining two directional reflectance parameters r_{sd} and r_{dd} can also be obtained and can be plotted. Thus, four directional reflectance parameters and six atmosphere parameters are derived and we modify these parameters to get the better results. Therefore, with these four directional reflectance parameters and six atmosphere parameters we obtain the total radiance that is received by the sensor.

To test the proposed imaging models, a scene with sparse rabbit brush and soil road is established and simulated. The scene, shown in Fig. 10.

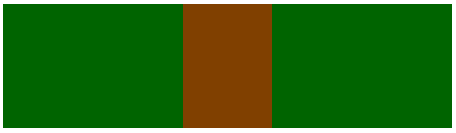

Fig 10 Simulation scene - Ideal scene

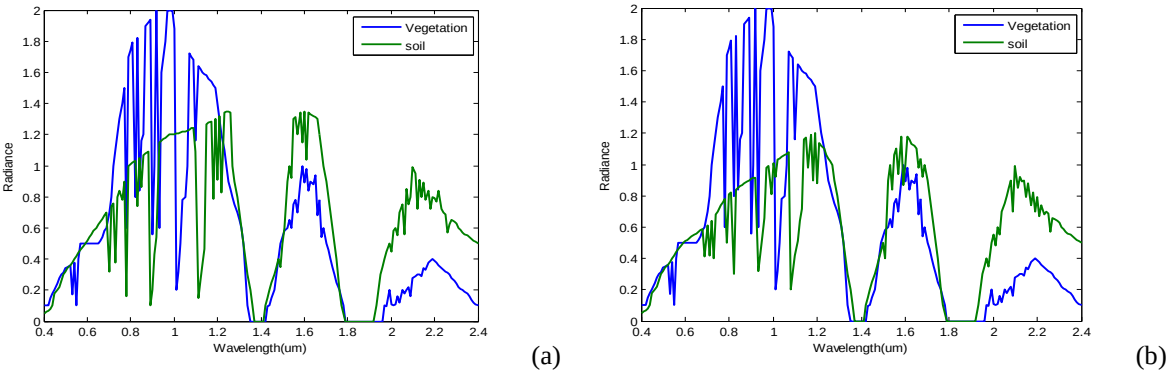

(a) (b)

Fig 11(a) maximum linear polarized radiances (b) minimum linear polarized radiances of vegetation and soil.

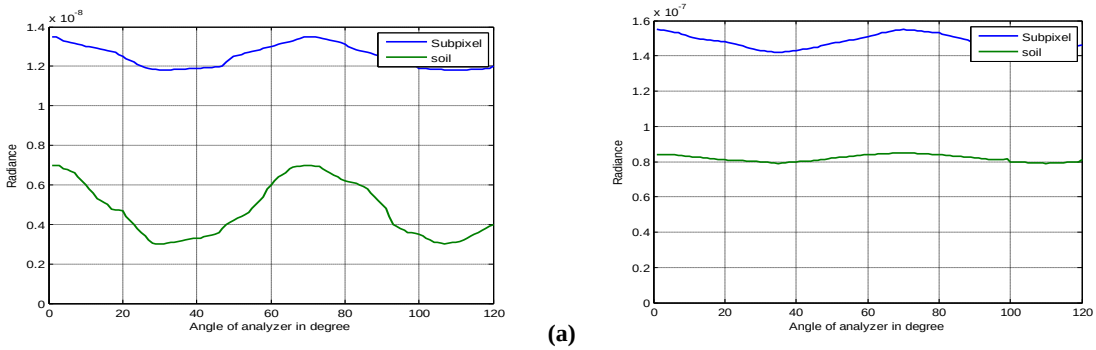

(a) (b)

Fig 12 Simulation of real scene (a) The polarized radiance at the 0.40 μm. (b) The polarized radiance at the 1.50 μm.

In Figure 13, the total radiance of the scene is the sum of maximum polarized radiance and minimum polarized radiance of the scene, and the polarized radiance of the scene is that maximum polarized radiance subtracts

ISSN: 2319-5967
ISO 9001:2008 Certified
International Journal of Engineering Science and Innovative Technology (IJESIT)
Volume 3, Issue 4, July 2014

minimum polarized radiance of the scene. As shown in Figure. 13 the polarization is different when the target is different, so the polarization plays similar role as spectral feature.

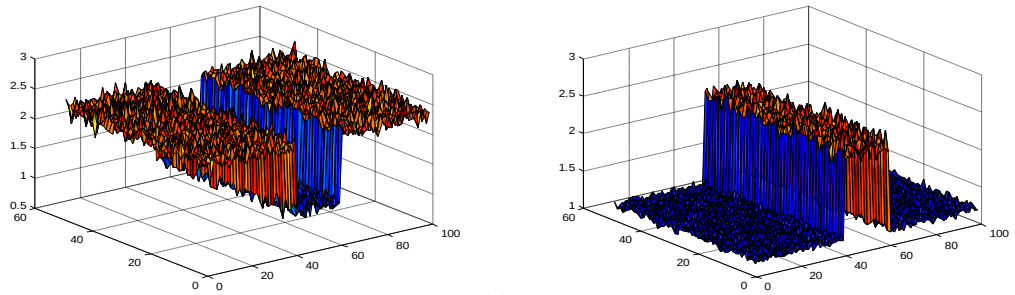

(a) (b)

Fig 13 Results of scene simulation at 0.40 μm. (a) The total radiance scene. (b) The polarized radiance scene.

V. FUTURE SCOPE

The outcome of the work help designers and users of a polarimetric hyper spectral imaging system to optimize sensor parameters and plan new missions. Polarimetric hyper spectral imaging can be used for growth monitoring of crops, analysis of water quality, and geology mapping, etc. The researches on polarimetric hyper spectral imaging mechanism and on image characteristics are of great importance for further information extraction and utilization of the images. The mapping of vegetation, water content is another emerging application for forest fire risk assessment, and forest defoliation resulting from heat waves, insect or fungus infections. In future more data modeling for better understanding of the interactions between the actively or naturally emitted radiance and the forest, a challenge is to understand interactions under various conditions.

VI. CONCLUSION

We study the polarimetric hyper spectral imaging model to realize the ideal and real scene implementation of polarimetric hyper spectral image. The Verhoef's six atmosphere parameters, and the influence of skylight on polarization is analyzed and four directional reflectance parameters are derived. Finally, we generate the polarimetric hyper spectral image data source according to the imaging model. The polarization can provide the supplementary information for the image interpretation other than spectral and spatial features. Polarimetric hyper spectral remote sensing combines the advantages of polarization and hyper spectral techniques. Polarization is different when the target is different so the Polarization is independent of the spectral feature. Spectral information can reveal the ground target's physical attribute and realize matching, classification, and discrimination, etc.

REFERENCES

[1]. A. Kuusk, "A multispectral canopy reflectance model," Remote Sens. Environ., vol. 50, no. 2, pp. 75–82, Nov. 1994.

[2]. G. Rondeaux and M. Herman, "Polarization of light reflected by crop canopies," Remote Sens. Environ., vol. 38, no. 1, pp. 63–75, Oct. 1991.

[3]. F. M. Bréon, D. Tanre, P. Lecomte, andM. Herman, "Polarized reflectance of bare soils and vegetation measurements and models," IEEE Trans. Geosci. Remote Sens., vol. 33, no. 2, pp. 487–490, Mar. 1995.

[4]. F. Maignan, F. M. Breon, E. Fedele, and M. Bouvier, "Polarized reflectances of natural surfaces: Space borne measurements and analytical modeling," Remote Sens. Environ., vol. 113, no. 12, pp. 2642–2650, Dec. 2009.

[5]. J. R. Shell, "Polarimetric remote sensing in the visible to near infrared," Ph.D. dissertation, Rochester Inst. Technol., Rochester, NY, 2005, pp. 1–259.

[6]. G. H. Suits, "The calculation of the directional reflectance of a vegetation canopy," Remote Sens. Environ., vol. 2, pp. 117–125, 1972.

[7]. W. Verhoef, "Light scattering by leaf layers with application to canopy reflectance modeling: The SAIL model," Remote Sens. Environ., vol. 16, no. 2, pp. 125–141, Oct. 1984.

[8]. W. Verhoef and H. Bach, "Simulation of hyper spectral and directional radiance images using coupled biophysical and atmospheric radiative transfer models," Remote Sens. Environ., vol. 87, no. 1, pp. 22–41, Sep. 2003.

[9]. A. Kuusk, "A fast, invertible canopy reflectance model," Remote Sens. Environ., vol. 51, no. 3, pp. 342–350, Mar. 1995.

ISSN: 2319-5967
ISO 9001:2008 Certified
International Journal of Engineering Science and Innovative Technology (IJESIT)
Volume 3, Issue 4, July 2014

[10]. T. Nilson and A. Kuusk, "A reflectance model for the homogeneous plant canopy and its inversion," Remote Sens. Environ., vol. 27, no. 2, pp. 157– 167, Feb. 1989.

[11]. F. Waquet, J.-F. Leon, B. Cairns, and P. Goloub, "Analysis of the spectral and angular response of the vegetated surface polarization for the purpose of aerosol remote sensing over land," Appl. Opt., vol. 48, no. 6, pp. 1228– 1236, Feb. 2009.

[12]. W. A. Allen, T. V. Gayle, and A. J. Richardson, "Plant canopy irradiance specified by the Duntley equations," J. Opt. Soc. Amer., vol. 60, no. 3, pp. 372–376, Mar. 1970.

[13]. J. Lenoble, M. Herman, and J. L. Deuze, "A successive order of scattering code for solving the vector equation of transfer in the earth's atmosphere with aerosols," J. Quant. Spectrosc. Radiat. Transf., vol. 107, no. 3, pp. 479–507, Oct. 2007.

[14]. S. Jacquemoud, W. Verhoef, F. Baret, C. Bacour, P. J. Zarco-Tejada, G. P. Asner, C. François, and S. L. Ustin, "PROSPECT+SAIL models: A review of use for vegetation characterization," Remote Sens. Environ., vol. 113, no. 1, pp. S56–S66, Sep. 2009.

[15]. V. C. Vanderbilt and L. Grant, "Plant canopy specular reflectance model," IEEE Trans. Geosci. Remote Sens., vol. GRS-23, no. 5, pp. 722–730, Sep. 1995.

[16]. F. Vachon, A. Royer, M. Aube, B. Toubbé, N. T. O'Neill, and P.M. Teillet, "Remote sensing of aerosols over North American land surfaces from POLDER and MODIS measurements," Atmos. Environ., vol. 38, no. 21, pp. 3501–3515, Jul. 2004.

[17]. A. Tonizzo, J. Zhou, and A. Gilerson, "Polarized light in coastal waters: Hyper spectral and multiangular analysis," Opt. Exp., vol. 17, no. 7, pp. 5666–5683, Mar. 2009.

[18]. J. Zhang, X. Zhang, B. Zou, and D. Chen, "On hyper spectral image simulation of a complex woodland area," IEEE Trans. Geosci. Remote Sens., vol. 48, no. 11, pp. 3889–3902, Nov. 2010.

[19]. V. C. Vanderbilt, "A model of plant canopy polarization response," Purdue Libraries, West Lafayette, IN, LARS Tech. Rep., pp. 98–108, 1980.

[20]. A. Ribes and F. Schmitt, "Linear inverse problems in imaging," IEEE Signal Process. Mag., vol. 25, no. 4, pp. 84–99, Jul. 2008.

[21]. J. P. Kerekes and D. A. Landgrebe, "Modeling, simulation, and analysis of optical remote sensing systems," School Elect. Eng., Purdue Univ., West Lafayette, IN, Tech. Rep. TR-EE 89-49, Aug. 1989.